High angular resolution visible light positioning using a quadrant photodiode angular diversity aperture receiver (QADA)

STEFANIE CINCOTTA,[1,*] CUIWEI HE,[1] ADRIAN NEILD,[2] AND JEAN ARMSTRONG[1]

[1]*Department of Electrical and Computer Systems Engineering, Monash University, Clayton, Australia*
[2]*Department of Mechanical and Aerospace Engineering, Monash University, Clayton, Australia*
Stefanie.Cincotta@monash.edu

Abstract: The increasing use of white LEDs for indoor illumination provides a significant opportunity for Visible Light Positioning (VLP). The challenge is to design a small, unobtrusive sensor that can be incorporated into mobile devices to provide accurate measurements for triangulation. We present experimental results for a novel angle of arrival (AOA) detector that has been designed for use in a VLP system. The detector is composed of a transparent aperture in an opaque screen that is located above a quadrant photodiode (PD), separated by a known vertical distance. Light passing through the aperture from an LED casts a light spot onto the quadrant PD. The position of this spot, coupled with knowledge of the height of the aperture above the quadrant PD, provides sufficient information to determine both the incident and polar angles of the light. Experiments, using a prototype detector, show that detector is capable of accurate estimation of AOA. The root mean square errors (rMSE) were less than 0.11° for all the measured positions on the test bed, with 90% of positions having an rMSE of less than 0.07°.

OCIS codes: (060.4510) Optical communications; (230.5160) Photodetectors; (050.1220) Apertures.

References and links

1. J. Armstrong, Y. A. Sekercioglu, and A. Neild, "Visible light positioning: a roadmap for international standardization," IEEE Commun. Mag., **51(**12), 68–73 (2013).
2. S.-Y. Jung, D.-H. Kwon, S.-H. Yang, and S.-K. Han, "Inter-cell interference mitigation in multi-cellular visible light communications," Opt. Express, **24**(8), 8512–8526 (2016).
3. Y. Xu, Z. Wang, P. Liu, J. Chen, S. Han, C. Yu and J. Yu, "Accuracy analysis and improvement of visible light positioning based on VLC system using orthogonal frequency division multiple access," Opt. Express, **25**(26), 32618–32630 (2017).
4. J. Luo, L. Fan, and H. Li, "Indoor Positioning Systems Based on Visible Light Communication: State of the Art," IEEE Commun. Surv. Tutor., **19**(4), 2871-2893 (2017).
5. N. Wu, L. Feng, and A. Yang, "Localization accuracy improvement of a visible light positioning system based on the linear illumination of LED sources," IEEE Photonics J., **9**(5), 7905611 (2017).
6. H. Steendam, T. Q. Wang, and J. Armstrong, "Theoretical Lower Bound for Indoor Visible Light Positioning Using Received Signal Strength Measurements and an Aperture-Based Receiver," J. Light. Technol., **35**(2), 309–319 (2017).
7. H. Zheng, Z. Xu, C. Yu, and M. Gurusamy, "A 3-D high accuracy positioning system based on visible light communication with novel positioning algorithm," Opt. Commun., **396**, 160–168 (2017).
8. T. Q. Wang, Y. A. Sekercioglu, A. Neild, and J. Armstrong, "Position Accuracy of Time-of-Arrival Based Ranging Using Visible Light With Application in Indoor Localization Systems," J. Light. Technol., **31**(20), 3302–3308 (2013).
9. T.-H. Do, J. Hwang, and M. Yoo, "TDoA-based indoor positioning using visible light," Photonic Netw. Commun., **27**(2), 80–88 (2014).
10. A. M. Vegni and M. Biagi, "An indoor localization algorithm in a small-cell LED-based lighting system," in *2012 International Conference on Indoor Positioning and Indoor Navigation (IPIN)*, 1-7 (2012).
11. S. H. Yang, H. S. Kim, Y. H. Son, and S. K. Han, "Three-Dimensional Visible Light Indoor Localization Using AOA and RSS With Multiple Optical Receivers," J. Light. Technol., **32**(14), 2480–2485 (2014).
12. A. Arafa, S. Dalmiya, R. Klukas, and J. F. Holzman, "Angle-of-arrival reception for optical wireless location technology," Opt. Express, **23**(6), 7755–7766 (2015).

13. L. Wei, H. Zhang, B. Yu, J. Song, and Y. Guan, "Cubic-Receiver-Based Indoor Optical Wireless Location System," IEEE Photonics J., **8**(1), 7390202 (2016).
14. Y.-S. Kuo, P. Pannuto, K.-J. Hsiao, and P. Dutta, "Luxapose: indoor positioning with mobile phones and visible light," in *Proceedings of the Annual International Conference on Mobile Computing and Networking (MOBICOM)*, 447–458 (2014).
15. M. H. Bergen, X. Jin, D. Guerrero, H. A. L. F. Chaves, N. V. Fredeen, and J. F. Holzman, "Design and Implementation of an Optical Receiver for Angle-of-Arrival-Based Positioning," J. Light. Technol., **35**(18), 3877–3885 (2017).
16. P. Huynh and M. Yoo, "VLC-Based Positioning System for an Indoor Environment Using an Image Sensor and an Accelerometer Sensor," Sensors, **16**(6), 783 (2016).
17. T. Q. Wang, C. He, and J. Armstrong, "Performance Analysis of Aperture-Based Receivers for MIMO IM/DD Visible Light Communications," J. Light. Technol., **35**(9), 1513–1523 (2017).
18. H. Steendam, T. Q. Wang, and J. Armstrong, "Cramer-Rao bound for indoor visible light positioning using an aperture-based angular-diversity receiver," in *2016 IEEE International Conference on Communications (ICC)*, 1-6 (2016).
19. H. Steendam, T. Q. Wang, and J. Armstrong, "Cramer-Rao bound for AOA-based VLP with an aperture-based receiver," in *2017 IEEE International Conference on Communications (ICC)*, 1-6 (2017).
20. I. Gőzse, "Optical Indoor Positioning System Based on TFT Technology," Sensors, **16**(1), 19 (2015).
21. S. Cincotta, A. Neild, C. He, and J. Armstrong, "Visible Light Positioning using an Aperture and a Quadrant Photodiode," in *2017 IEEE Globecom Workshops*, 1-6 (2017).
22. H. Steendam, "A 3D Positioning Algorithm for AOA-Based VLP with an Aperture-Based Receiver," IEEE J. Sel. Areas Commun., **36**(1), 23–33 (2017).
23. J. H. G. Huisstede, K. O. van der Werf, M. L. Bennink, and V. Subramaniam, "Force detection in optical tweezers using backscattered light," Opt. Express, **13**(4), 1113–1123 (2005).
24. A. M. Nugrowati, W. G. Stam, and J. P. Woerdman, "Position measurement of non-integer OAM beams with structurally invariant propagation," Opt. Express, **20**(25), 27429–27441 (2012).
25. J. M. Kahn and J. R. Barry, "Wireless infrared communications," Proc. IEEE, **85**(2), 265–298 (1997).
26. A. Haapalinna, P. Kärhä, and E. Ikonen, "Spectral reflectance of silicon photodiodes," Appl. Opt., **37**(4), 729–732 (1998).
27. A. Arafa, X. Jin, and R. Klukas, "Wireless Indoor Optical Positioning With a Differential Photosensor," IEEE Photonics Technol. Lett., **24**(12), 1027–1029 (2012).

1. Introduction

Demand is increasing for a reliable and economical indoor positioning system [1]. Visible light positioning (VLP), using the new receiver we describe in this paper, has the potential to meet this demand. Recent research has shown that VLP using lighting LEDs can provide extremely accurate indoor positioning information and the increasing uptake of energy efficient LED lighting means that VLP has the potential to become a ubiquitous technology [2], [3]. VLP is based on visible light communication (VLC). In VLC, the light transmitted by the LEDs in luminaires is modulated and used to transmit data. In the case of visible light positioning (VLP), the luminaires transmit information about their position and so act as beacons in a positioning system. Receivers, using photodiodes (PDs) or image sensors, can detect these signals and use them to determine the position of the receiver.

Many different approaches to VLP have been described in the literature [4]. These include techniques based on received signal strength, time of arrival, time difference of arrival, fingerprinting, and angle of arrival (AOA). A number of theoretical and experimental papers have shown that in particular circumstances each of these methods can provide accurate positioning, but each has significant disadvantages.

Received signal strength [5]–[7] is a popular and relatively straightforward method in which the power of the received signal is used to estimate the distance between the transmitter and the receiver. The main limitation of received signal strength is that it relies on accurate knowledge of the radiation pattern of the transmitter, the channel, and the transmitted power. In practice these may be difficult to ascertain and may change over time. Time of arrival [8] and time difference of arrival [9], depend on measuring the times of arrival of signals from different transmitters. Time difference of arrival is very successfully employed in GPS, but an accurate atomic clock is required in each GPS transmitter and all the clocks must be precisely synchronized in order to measure the time differences. This is unsuitable for VLP due to the additional expensive infrastructure and the difficulty in measuring extremely small time

differences. The disadvantage of fingerprinting methods is that, before any positioning can take place, measurements must be made and stored for known positions throughout the scenario [10].

AOA systems depend on measuring the angle of arrival of signals from a number of different transmitters and using this information for triangulation-based positioning. Appealingly, the transmitters need not be synchronized or of known power. The challenge for AOA systems is the design of suitable angular diversity receivers. A number of different receivers have achieved this, either using PDs [11]–[13] or cameras [14]–[16]. Many of those using PDs have three dimensional structures with the PDs facing in different directions. In [11], tilted PDs in a pyramidal type structure are used, while in [12] a cubic receiver is described. The practical disadvantage of these structures is that they cannot be easily incorporated into smart devices such as modern mobile phones. If VLP is to be extensively used, receivers must be developed that are both compact and planar. The angular diversity aperture (ADA) receiver [17], whilst designed for VLC, does meet these requirements and theoretical and simulation results have shown that accurate positioning is possible [6], [18], [19]. The original ADA receiver used multiple receiving elements each consisting of an aperture and a photodiode. Most work so far on their use in VLP is theoretical and assumes that the size and position of each receiving element is accurately known and that the photodiodes have precisely matched characteristics. A completely different approach that uses an aperture is described in [20] where a thin film transistor (TFT) unit was used to create an aperture that can be used for tracking a light beacon.

In this paper we analyze and present the first experimental validation of a new type of ADA receiver that uses a quadrant PD and a single aperture. This new design removes the requirements for accurate matching between different photodiodes and accurate positioning of multiple apertures and photodiodes. In addition, this new receiver can accurately detect AOA over a wide FOV whilst maintaining a compact structure [21]. Experimental results demonstrate very high accuracy from this detector, making it ideal for use in future VLP systems.

2. System description

The ADA receiver, using multiple apertures and discrete PDs, was initially developed for VLC multiple-input multiple-output (MIMO) systems [17], but was later shown, theoretically, to be effective for VLP [6], [22]. In this paper, we describe the new quadrant photodiode ADA (QADA) receiver which has been designed specifically for VLP. To enable practical operation, it uses a single aperture and a quadrant PD to create an AOA detector.

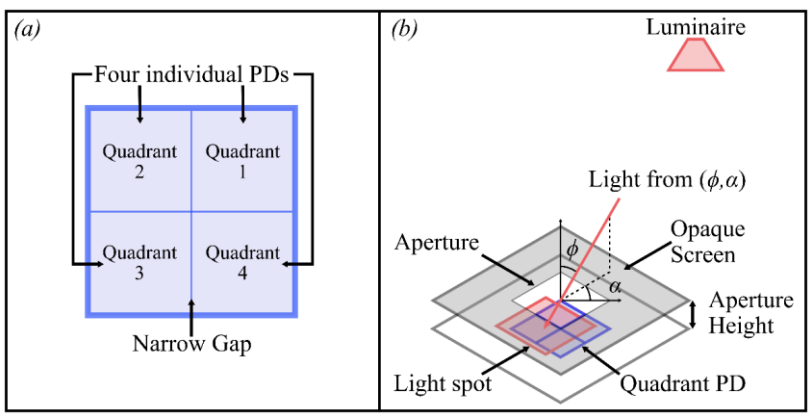

Fig. 1. (a) Quadrant PD showing individual quadrants and narrow gap, and (b) Receiver structure with received light spot overlapping the quadrant PD

Quadrant PDs are made up of four individual PDs, separated by a narrow gap, shown in Fig. 1(a). They offer position detection in two dimensions. Previously, they have been used for beam centering and other well-known laser light applications [23], [24]. The key features of our new design is that we use an aperture and that the aperture is located at a known height above the quadrant PD. The aperture is required because the light source in our new application is diffuse. The aperture is used to form a well-defined beam of light that falls on the quadrant PD. The aperture is located at a known height above the quadrant PD as this provides the additional information necessary to calculate the AOA.

We have designed an algorithm that estimates the position of the center of the light spot overlapping the quadrant PD. This information, combined with the height of the aperture, gives both the incident and polar angles of the received light. These angles can then be used with a triangulation algorithm to determine the location of the receiver.

2.1 Concept behind the QADA receiver

The new detector, shown in Fig. 1(b), consists of a quadrant PD located directly below a transparent aperture in an opaque screen. Light passing through the aperture casts a light spot onto the quadrant PD. The position of the light spot is unique for a given AOA, thus, accurately estimating the position of the light spot gives information that is then used to calculate the AOA of the light from the luminaire.

For maximum positioning information, the light spot must overlap all four quadrants of the PD. The vertical distance between the aperture plane and the photodiode plane, termed the aperture height, determines the field of view (FOV) of the detector. As the height becomes larger, the FOV becomes smaller. Because the aperture height is fixed for a given design, it can be combined with the detected displacement of the light spot from the center of the quadrant PD to determine the incident and polar angles.

The aperture and quadrant PD can be any shape desired. However, an important advantage of using a square aperture is that it results in a proportional linear change in the overlap areas of the quadrants as the light spot moves across the detector; this substantially simplifies the algorithm needed to detect position. The size of the light spot is determined by the aperture size. Ideally, the aperture size and shape matches that of the PD as this maximizes the area of the light spot and consequently the strength of the detected signals. However, so long as the light spot is not larger than the quadrant PD, overlaps all four photodiode elements and is not smaller than the gap between quadrants, there will be no ambiguity in position detection.

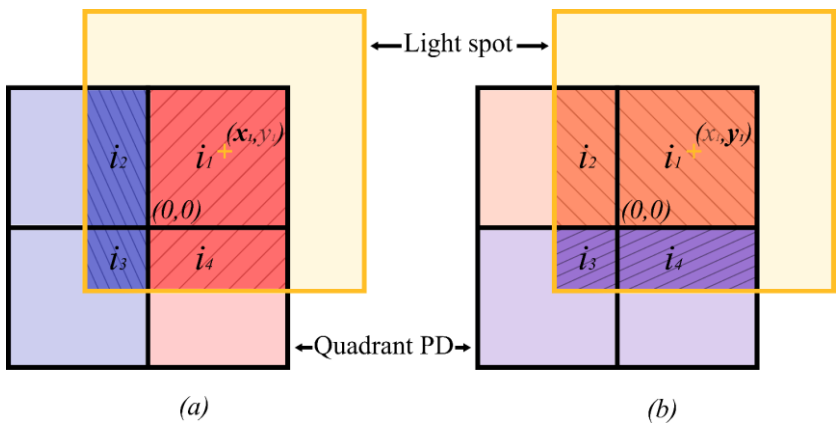

Fig. 2. Light spot, shown in yellow, overlapping a quadrant PD. In (a) we show how the displacement in *x* is determined using the photocurrents from the left and right quadrant pairs. In (b), we show how the displacement in *y* is determined using the photocurrents from the top and bottom quadrant pairs.

2.2 Algorithm

We initially analyze the ideal case of a square quadrant PD and a square aperture of the same size. To determine position of the receiver, we need to know the displacement of the light spot center from the center of the quadrant PD. In the general case, the receiver is moving and the light spot will vary with time. Thus, we must determine $\left[x_1(t), y_1(t)\right]$, the position of the light spot center at time, t.

The algorithm we have developed to detect the position of the light spot center uses the ratio of the photocurrents generated by adjacent pairs of quadrants. The ratio between the received photocurrents from the left and right quadrant pairs can be used to find displacement in the x direction, shown in Fig. 2(a). Similarly, the ratio between the received photocurrents from the top and bottom quadrant pairs can be used to find displacement in the y direction, shown in Fig. 2(b). These ratios can be expressed as

$$p_x(t) = \frac{i_1(t) + i_4(t) + N_1(t) + N_4(t)}{i_2(t) + i_3(t) + N_2(t) + N_3(t)} \tag{1}$$

$$p_y(t) = \frac{i_1(t) + i_2(t) + N_1(t) + N_2(t)}{i_3(t) + i_4(t) + N_3(t) + N_4(t)} \tag{2}$$

where $i_j(t)$ and $N_j(t)$ are the photocurrent and noise from the j^{th} quadrant, after filtering, at time, t.

The photocurrent generated in each quadrant is proportional to the received optical power, which is dependent on the light spot overlap area. In the absence of noise, the ratios, $p_x(t)$ and $p_y(t)$, can be reduced to ratios of overlap areas, where the areas are a function of the length of the PD quadrant, L_{PD}, and the position of the light spot. Thus, (1) can be expressed as

$$p_x(t) = \frac{A_1(t) + A_4(t)}{A_2(t) + A_3(t)} == \begin{cases} \dfrac{L_{PD} + x_1(t)}{L_{PD}}, & -L_{PD} < x_1(t) \le 0 \\ \dfrac{L_{PD}}{L_{PD} - x_1(t)}, & 0 < x_1(t) < L_{PD} \end{cases} \tag{3}$$

where $A_j(t)$ is the area the light spot overlaps with the j^{th} quadrant of the PD, at time t. And, using symmetry, a similar expression for Eq. (2) can be derived. We can now rearrange Eq. (3) to give

$$x_1(t) = \begin{cases} L_{PD}\left(p_x(t) - 1\right), & -L_{PD} < x_1(t) \le 0 \\ L_{PD} - \dfrac{L_{PD}}{p_x(t)}, & 0 < x_1(t) < L_{PD} \end{cases} \tag{4}$$

which we use to derive an estimate for $x_1(t)$.

From Eq. (3), it can be seen that the ratio, $p_x(t)$, is independent of the value of $y_1(t)$. However, the individual photocurrents, $i_j(t)$, are not. Consequently, when $y_1(t) \neq 0$ the signal to noise ratio (SNR) will be reduced.

We consider the case where the estimate is calculated in the digital domain and the received signal is low-pass filtered in the electrical domain to limit the bandwidth to B hertz. It is then

sampled at the Nyquist rate, $2B$, and averaged over M samples so that the estimate at time $t=\left(k+M\right)/2B$ is given by

$$\hat{x}_1\left[\frac{k+M}{2B}\right]=\begin{cases}\dfrac{1}{M}\displaystyle\sum_{n=k}^{k+M-1}L_{PD}\left(p_x\left[\frac{n}{2B}\right]-1\right), & -L_{PD}<x_1\left[\dfrac{k+M}{2B}\right]\le 0\\ \dfrac{1}{M}\displaystyle\sum_{n=k}^{k+M-1}L_{PD}-\frac{L_{PD}}{p_x\left[\dfrac{n}{2B}\right]}, & 0<x_1\left[\dfrac{k+M}{2B}\right]<L_{PD}\end{cases} \tag{5}$$

2.3 Noise analysis

We now consider the impact of noise on the system. We develop an expression for the algorithm in the presence of noise and demonstrate how the resultant noise terms in the ratio function, $p_x(t)$, vary with both the AOA of the light and the vertical distance between the transmitter and receiver.

If we assume the LED is emitting a Lambertian radiation pattern, the general expression for the DC channel gain at time, t , for the j^{th} quadrant of the PD is given by [25]

$$h_c(t)=\frac{(m+1)A_j(t)}{2\pi d^2(t)}\cos^m\left(\phi(t)\right)T_s\left(\psi(t)\right)g\left(\psi(t)\right)\cos\left(\psi(t)\right) \tag{6}$$

where m is the Lambertian order of the LED, $T_s(\psi)$ is the transmission of the filter, $g(\psi)$ is the concentrator gain, ϕ and ψ are the emergence and incidence angles respectively and d is the distance between the transmitter and receiver. If we restrict our analysis to the case where there is no concentrator or filter, the Lambertian order of the LED is one, and the receiver is pointing straight up at the transmitter so that the incidence and emergence angles are equal, we can then define the photocurrent at time, t , for the j^{th} quadrant as

$$i_j(t)=\frac{RP_TA_j(t)\cos^2\left(\psi(t)\right)}{\pi d^2(t)} \tag{7}$$

The dominant noise source in an optical wireless system is the shot noise induced by the background illumination [25]. This light is isotropic, however because we use an aperture, the background light reaching the quadrant PD is reduced. Thus, the following analysis will lead to an overestimation of the noise.

We model the shot noise as a white Gaussian process with single-sided noise power density given by

$$N_0=2qRp_nA\Delta\lambda \tag{8}$$

where q is the charge of an electron, R is the responsivity of the PD, p_n is the spectral irradiance, A is the area of a single quadrant of the PD and $\Delta\lambda$ is the bandwidth of the optical filter. Thus, the variance of the noise will be the product of the single sided noise power density and the electrical bandwidth, B .

$$\sigma_n^{\,2}=N_0B \tag{9}$$

For the case where $y_1(t)=0$, substituting Eqs. (7) and (9) into Eq. (1), gives:

$$p_x(t)=\begin{cases}\dfrac{2k_1\cos^4\left(\psi(t)\right)L_{PD}{}^2+2k_1\cos^4\left(\psi(t)\right)L_{PD}x_1(t)+N_1(t)+N_4(t)}{2k_1\cos^4\left(\psi(t)\right)L_{PD}{}^2+N_2(t)+N_3(t)} \\ \quad=\dfrac{L_{PD}+x_1(t)+E_1(t)}{L_{PD}+E_2(t)}, \quad -L_{PD}<x_1(t)\le 0 \\ \dfrac{2k_1\cos^4\left(\psi(t)\right)L_{PD}{}^2+N_1(t)+N_4(t)}{2k_1\cos^4\left(\psi(t)\right)L_{PD}{}^2-2k_1\cos^4\left(\psi(t)\right)L_{PD}x_1(t)+N_2(t)+N_3(t)} \\ \quad=\dfrac{L_{PD}+E_1(t)}{L_{PD}-x_1(t)+E_2(t)}, \quad 0<x_1(t)<L_{PD}\end{cases} \tag{10}$$

where $k_1=\left(RP_t/\pi\right)$ is a constant value. The noise terms, $E_1(t)$ and $E_2(t)$, have zero mean and a variance of:

$$\begin{aligned}\sigma_e(t)^2&=\left(\frac{1}{2k_1\cos^4\left(\arctan\left(\sqrt{x_1(t)^2+y_1(t)^2}/h\right)\right)L_{PD}}\right)^2\times 2\sigma_n{}^2 \\ &=\frac{\pi^2\left(H+h\right)^4 qp_nA\Delta\lambda B}{RP_T{}^2L_{PD}{}^2\cos^8\left(\psi(t)\right)}\end{aligned} \tag{11}$$

H is the vertical distance between the transmitter and receiver and h is the vertical distance separating the aperture and the quadrant PD. From Eq. (11), it can be seen that an increase in the electrical filter bandwidth, B, will result in decreased performance as the variance of the noise term is directly proportional to this value.

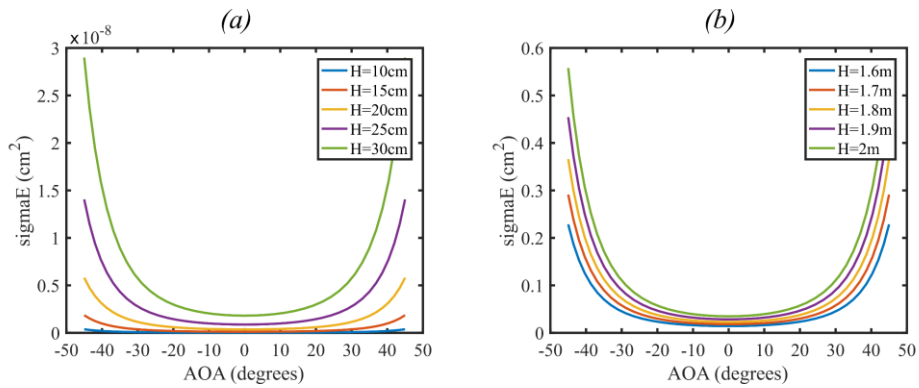

Fig. 3. $\sigma_e{}^2$ for varying AOA and varying vertical distance, *H*, between the transmitter and the receiver, (a) shows the values of *H* used in the experiment and (b) shows more typical values of *H* that are encountered in positioning applications. The variance is larger for large arrival angles and large values of *H* due to the reduced received optical power.

In Fig. 3, $\sigma_e{}^2$ is plotted for varying AOA and vertical distance. In both plots, it can be seen that the magnitude of $\sigma_e{}^2$ is worse for large arrival angles and for large values of H. This is due to the reduced optical power received when the distance separating the transmitter and receiver is increased. The parameters used for this simulation are shown in Table 1.

Table 1. Simulation parameters

Parameter	Value
Power transmitted (P_t)	3 W
Responsivity (R) (@ 440 nm)	0.15 A/W
Optical filter bandwidth ($\Delta\lambda$)	300 nm
Electrical filter bandwidth (B)	1 MHz
Spectral irradiance (p_n)	6.2 x 10^6 W/(nm·cm^2)
Length of PD (L_{PD})	2 mm
Aperture height (h)	2 mm

3. Experiment

The block diagram of the experiment is shown in Fig. 4. The transmitter, shown in the red box, was a white LED (Luxeon LXML-PWC2) emitting a 200 kHz sine wave. The signal, provided by an arbitrary waveform generator (AWG, Tektronix 3022B), was amplified by a power amplifier (Mini-circuits ZHL-32A-S) before adding a DC bias using a bias-T (Mini-circuits ZFBT-4R2GW).

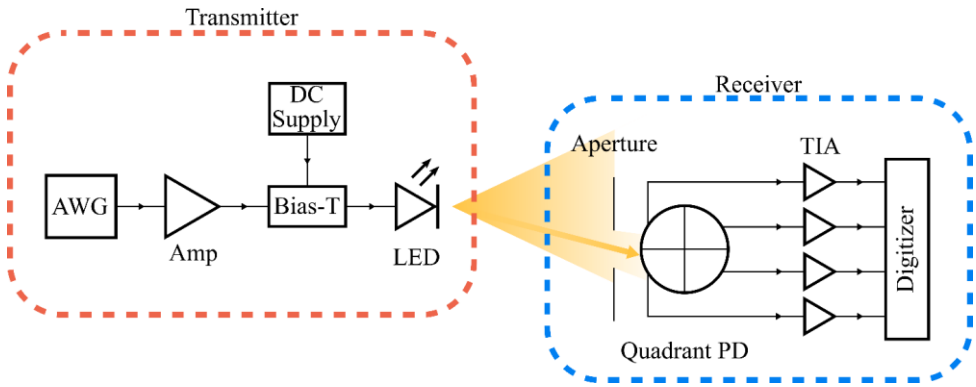

Fig. 4. Block diagram of the experimental set-up. The transmitter circuit, shown on the left, drives a white LED that outputs a 200 kHz sine wave. The light from the LED passes through the aperture and is received by the quadrant PD, shown on the right. It is then amplified and captured by a digitizer.

The receiver, shown in the blue box, consisted of the quadrant PD and an aperture. To optimize the performance, the quadrant PD was operated in photovoltaic mode with no bias. The output of each quadrant of the PD was connected to a transimpedance amplifier (Femto DHPCA-100) before the signals were captured by a digitizer (GaGe CSE8389). The data was analyzed in MATLAB to determine the receiver position.

The experiment was performed on an optical table, shown in Fig. 5, with two perpendicular optical rails, each with a linear stage. The receiver, in the blue box, was mounted on one of the linear stages and the transmitter, in the red box, was mounted on the other. This set-up allowed for the capture of data in varying positions in two dimensions.

The quadrant PD was attached to a breakout board and held in place using a custom 3D printed bracket. In front of the quadrant PD an XY translation mount was used to hold another custom 3D printed bracket that contained the aperture.

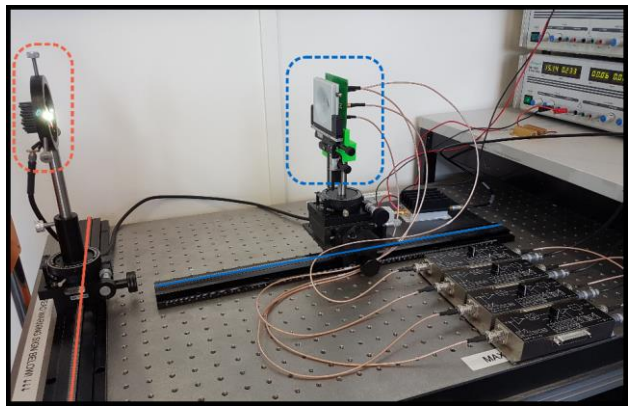

Fig. 5. Photograph of the experiment. The transmitter, in the red box, moves along the optical rail that is highlighted in red. The receiver, in the blue box, moves along the optical rail that is highlighted in blue.

3.1 Experimental algorithm

For this experiment, we selected a readily available circular quadrant PD (OSI SPOT-9DMI) with a diameter of 10 mm. Located directly in front of the quadrant PD was a 4mm square aperture. The distance separating the aperture and the quadrant PD was 2.25 mm. In order to maintain the linear relationship between the movement of the light spot and the change in overlap areas, it was optimal to use a square aperture with a side length that was smaller than the diameter of the quadrant PD.

We replace the general algorithm in Eq. (3) with one that has been designed for this geometry of PD and aperture:

$$p_x(t) = \frac{L_{ap} + x_1(t)}{L_{ap} - x_1(t)}, \quad -L_{ap} \le x_1(t) \le L_{ap} \tag{12}$$

where L_{ap} is half the side length of the aperture. From Eq. (12), we get

$$x_1(t) = \frac{L_{ap}(p_x - 1)}{(1 + p_x)}, \quad -L_{ap} \le x_1(t) \le L_{ap} \tag{13}$$

which can be used to derive an estimate for $x_1(t)$.

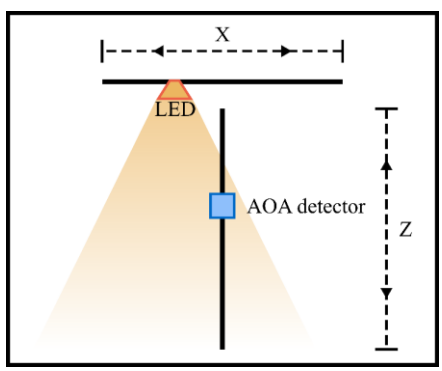

Fig. 6. Schematic showing possible movement of transmitter and receiver

3.2 Calibration

Due to the accuracy of the receiver, the experimental set up needed to be carefully aligned. To this end, the calibration of the receiver was performed in several steps. The first step aligned the receiver with the transmitter to find the zero position on the *x*-axis. This was performed without an aperture. The LED transmitter was moved along the *x*-axis, shown in Fig. 6, until the sums of the photocurrents from the left and right quadrants were equal. The height of the transmitter was then adjusted until the sums of the photocurrents from the top and bottom quadrants were equal. Next, the aperture was aligned with the quadrant PD using the XY translation mount and the rotation screw in the 3D printed bracket. Similar to the previous step, adjustments were made until all photocurrents were equal. Finally, the transmitter was moved 5 cm to the left and 5 cm to the right with measurements taken at both positions. These values were used to determine if there was any rotation about the *y*-axis. The receiver was then rotated until these results were symmetric. Note that this calibration is to ensure accuracy in our measurement system, so that we know what the exact angle is and compare that to what is measured, it would not be required in a real system.

3.3 Results

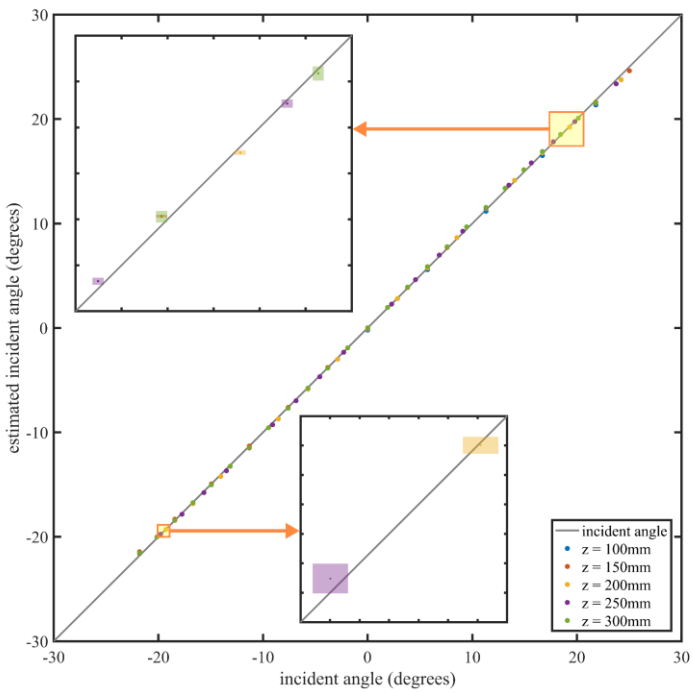

Fig. 7. Estimated incident angle vs true incident angle for all measured positions, demonstrating the accuracy of the QADA. The color patches represent error bars of one standard deviation. Insets at different magnifications for clarity.

Measurements were taken in one centimeter increments along the *x*-axis and five centimeter increments along the *z*-axis. Figure 7 shows the close correlation between the experimental estimated incident angle and the true incident angle. The largest error in estimation of the incident angle was 0.46° and this occurred when the magnitude of the incident angle was highest. Over 90% of the errors in incident angle estimation were below 0.25°.

Figure 8 shows the root mean square error (rMSE) in detection of the incident angle for varying distances. The maximum rMSE was 0.1077° and the minimum was 0.0054°. Over 90% of rMSE were less than 0.07°. As expected, the rMSE are worst when the distance along the *z*-axis is largest. This is as expected as, from (11), we can see that the variance on the measurement of the position of the light spot is directly proportional to the fourth power of *H*, the distance between transmitter and receiver. In this experiment the distance along the *z*-axis is analogous to the height. The rMSE also increases as the magnitude of the incident angle increases. This is due to the reduction in received optical power for increasing incident angle.

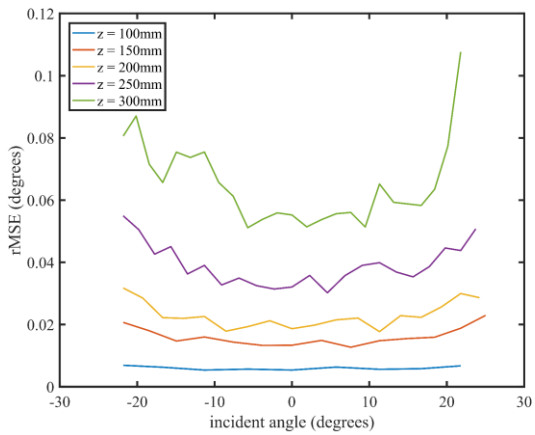

Fig. 8. Experimental results showing root mean square error for varying AOA

4. Discussion

The experimental results we have presented in this paper, using off-the-shelf components and a manual calibration method, demonstrate the accuracy of the detector. Figure 9 shows the experimental results for rMSE plotted on the same graph as the simulation results. The simulation used realistic parameters that were similar to those used in the experiment. It can be seen that there is a very close correlation between simulation and experimental results with the experimental results being slightly worse, as expected. This is probably due to calibration difficulties, combined with the simplified assumptions that are modelled in the simulation. For example, it is unlikely that the LED was a truly perfect Lambertian transmitter. The reduction in FOV for the experimental results is due to the reflectivity of the silicon [26] and the impact of Snell's law, which degrade the results for large incident angles. As both the thickness and refractive index of the glass in the quadrant PD packaging were unknown, it was not possible to correct for the refractive errors.

Due to the precision required to make accurate measurements that were suitable for meaningful comparison with simulation, calibration posed a significant difficulty for this experiment. Most of these calibration difficulties will not be present in a commercial implementation. It is likely that mass fabrication of such a detector will only require a factory calibration step to determine any alignment issues between the quadrant PD and the aperture. Any imperfections found will be corrected for in software. Additionally, the detector should be protected from the atmosphere with a transparent layer built into the structure. Any refractive index introduced by this layer will also need factory calibration and to be accounted for in software.

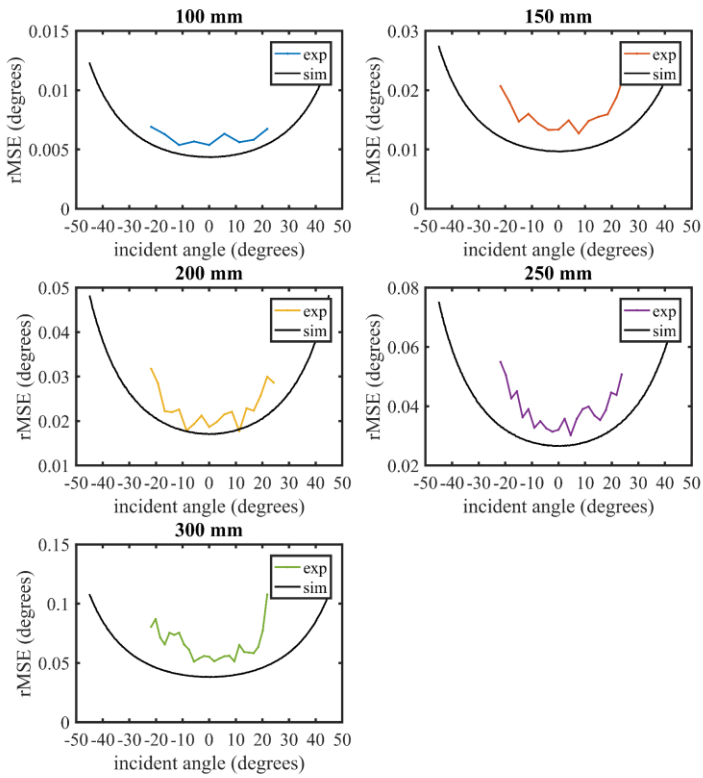

Fig. 9. Simulation and experimental results for root mean square error in incident angle detection. The experimental results, shown in colour, are closely matched to the simulation results, shown in black.

Compared to other AOA detectors that have experimental results published, the QADA receiver has superior performance. In [27], a cubic receiver was able to achieve errors, for the detection of incident angle, in the range of 0.7° – 6.8° and in [13] a different cubic receiver reported errors between 1° and 1.4° in detection of incident angle. Not only are the results for the QADA receiver better (all errors in incident angle detection are less than 0.5°), the QADA receiver has the important advantage of having a thin planar structure which is easier to incorporate into current consumer electronics. Other AOA systems that use cameras are able to achieve high levels of accuracy [15]. However, they have the disadvantages of either needing high frame rates, which add significant expense, or complex algorithms. They also consume a lot of power. By comparison, the QADA receiver is a simple and low power device that can be constructed using relatively cheap components, and clearly meets the requirements for widespread integration.

5. Conclusion

We present analytical and experimental results for our proposed QADA receiver. The results demonstrate that the QADA can support very accurate indoor positioning with centimetre accuracy in typical rooms. A key feature of the QADA is its compact planar structure. Our experiments used an off-the-shelf quadrant PD in a QADA receiver with dimensions compatible with incorporation in a compact portable device like a smart phone. Our

experimental results very closely matched our theoretical predictions. These results show that, with rMSE errors less than 0.11°, in addition to being more compact than some of the three dimensional receivers that have previously been described, the QADA is also more accurate. We have demonstrated that the new QADA receiver has the potential to form a key component of future indoor positioning systems.

Funding
This work was supported by the Australian Research Council's (ARC) Discovery funding schemes (DP130101265), (DP150100003) and an Australian Government Research Training Program (RTP) Scholarship.